筑　波　大　学
University of Tsukuba

博　士　（人間生物学）　学　位　論　文
Ph.D. dissertation in Human Biology

Elucidation of the involvement of REM sleep in cerebral blood flow regulation and its molecular mechanism
(レム睡眠による脳血流制御への関与およびその分子機構の解明)

2020

筑波大学グローバル教育院

School of Integrative and Global Majors in University of Tsukuba

Ph.D. Program in Human Biology

Chia-Jung Tsai

TABLE OF CONTENTS

ACKNOWLEDGEMENT

I would like to express my deep gratitude to my supervisor Dr. Hayashi for allowing me to join his laboratory at International Institute of Integrative Sleep Medicine (IIIS), for his motivation, patience, immense knowledge and his continuous supports of my Ph.D. research. Dr. Hayashi is a talented mentor who often inspires me with exciting ideas, in the meantime, he always respects my opinions and leaves room for challenging myself while open for discussion anytime. I could not imagined accomplishing this doctoral thesis without his tremendous instructions. I have learnt a lot from this mentorship, especially Dr. Hayashi's knowledge and philosophy of science during these 5 years of doctoral study.

I would also like to give my sincere appreciation to the following people who are indispensable in this doctoral study: Dr. Masashi Yanagisawa for providing the two-photon microscope and many valuable advice in my study. Dr. Kaspar Vogt for his patient and excellent instructions on mouse craniotomy surgery and teaching me the basic knowledge about composing a MATLAB program to analyze EEG and EMG data. Dr. Takeshi Kanda and Mr. Takehiro Miyazaki for maintaining the two-photon microscope and polysomnography recordings, so I can efficiently perform two-photon imaging without troubles. Dr. Takeshi Nagata for his instructions, discussions, and collaboration in composing MATLAB programs used in analyzing two-photon imaging data, which greatly speeded up the analysis procedures. Dr. Michael Lazarus, Dr. Tsuyoshi Saito and Dr. Hiroshi Nagase for providing *$A_{2A}R$*-KO mice and A_{2A}R PAM-1 for me to conduct the experiments. Dr. Chih-Yao Liu for his instructions in conducting mouse surgery of EEG and EMG electrode implantation and sleep recording, as well as his help in carrying out the blind tests for my experiment. Ms. Nanae Nagata for her instructions on performing the flowerpot method of sleep disturbance in mice.

Last but not the least, I would like to thank my families: my grandparents, my parents, my sister and my partner for spiritual supporting throughout my study in Japan and writing this thesis.

ABSTRACT

Mammalian sleep comprises two distinct stages, rapid eye movement (REM) sleep and non-REM (NREM) sleep. Various drastic changes occur during NREM sleep are considered as regenerative function of sleep, in contrast, much less is known about the physiological changes during REM sleep. Cerebral blood flow (CBF) is critical in maintaining energy-dependent processes and clearance of metabolic byproducts generated by neuronal activity. Impaired CBF regulation can affect numerous biological functions and CBF dysregulation also showed correlated with neurodegenerative disorders such as Alzheimer's Disease. CBF is strictly and independently regulated from the peripheral circulation. Till now, various approaches have been taken to investigate CBF dynamics across wake/sleep, but the results remained ambiguous. According to studies using positron emission tomography, global CBF is decreased during NREM sleep and comparable to the awake level during REM sleep, whereas according to studies using ultrasonic techniques, the CBF is highest during REM sleep. These conflicts are likely due to differences in the data processing and normalization procedures as well as differences in the type of blood vessels that are observed. To overcome these problems, I developed an alternative approach using two-photon microscopy imaging to directly measure the movement of individual red blood cells within capillaries, where actual substances exchange between blood and neurons/glia occurs, across wake/sleep cycle. As a result, I found that capillary CBF was largely elevated during REM sleep, whereas CBF during NREM sleep was comparable to the awake level across multiple cortices. Furthermore, at the molecular level, signaling via adenosine A_{2A} receptor was crucial for capillary CBF upsurge during REM sleep. The results should provide a final conclusion on how CBF changes during sleep, and provide critical evidence on how REM sleep contributes to maintaining our health.

INTRODUCTION

Introduction of mammalian sleep

Sleep is a distinct physiological state which occurs periodically in daily life and accounts for one-third of our lifetime. The feature of sleep is behavioral quiescence typically characterized by decreased locomotion activity, reduced consciousness, elevated arousal threshold to outer stimuli, rapid reversibility, and is homeostatically regulated (Miyazaki et al., 2017). In addition to behavioral characteristics, there are electrophysiological, molecular and pharmacological criteria to define sleep. Although these sleep criteria have not yet been examined upon a broad scope of animals, some criteria are species-specific. Mammalian sleep is composed of two distinct stages, rapid eye movement (REM) sleep (when people claim to have vivid dreams) and non-rapid eye movement (NREM) sleep. REM sleep has only been observed in various mammalian, avian, and perhaps some reptilian species so far, but not in other vertebrates (Campbell and Tobler, 1984; Rial et al., 2010).

Electroencephalograms (EEG) and electromyograms (EMG) can be used to distinguish sleep stage and wakefulness easily. During wakefulness, the EEG is dominated with low amplitude and high-frequency activity, as well as high muscle activity evident in the EMG. Awake EEG and the EEG in REM sleep show similar patterns, but REM sleep can be easier distinguished from wakefulness by low EMG signal since animals lose muscle tone during REM sleep. EEG in REM sleep dominated with theta activity with a defined frequency of 6 to 10 Hz. NREM sleep is generally followed by REM sleep in a repeating cycle. During NREM sleep, highly synchronized hyperpolarization activity from cortical neurons results in high amplitude slow wave (or delta wave) detected in the EEG with a defined frequency of 0.5 to 4 Hz.

Neurochemical mechanism of sleep regulation

The fact that sleep is homeostatic rebound to sleep deprivation implies that there are some physiological mechanisms involved in monitoring the sleep needs and keep tracks on the sleep debt. Adenosine is a nucleoside neuromodulator and plays a role in sleep regulation. The level of adenosine is influenced by neural activity since it is a secondary by-product of the ATP and cAMP breakdown. Extracellular adenosine concentration increases with brain metabolism, which in turn inhibits cholinergic neurons in the forebrain that promote wakefulness. Therefore, the accumulation of adenosine during prolonged wakefulness might serve as sleep-promoting substances (Porkka-Heiskanen et al., 1997). It is also known that

caffeine induces wakefulness through binding to adenosine A_{2A} receptors as an antagonist (Huang et al., 2005).

Acetylcholine is an important neurotransmitter involved in arousal. Microdialysis analysis revealed that the levels of acetylcholine were high during wakefulness and REM sleep when EEG show desynchronized activity, but low in NREM sleep (Marrosu et al., 1995). Electrical stimulation of cholinergic neurons in the brain stem increases the release of acetylcholine and promotes REM sleep (Lydic and Baghdoyan, 1993; Thakkar et al., 1996).

It is also known that monoamines promote wakefulness, for example, serotonin (5-HT)-containing neurons of dorsal ráphe nucleus, norepinephrine-containing neurons of locus coeruleus, and histamine-containing neurons of the tuberomammillary nucleus fire at their fastest rate during wakefulness, and decline when entering NREM sleep, while ceasing firing during REM sleep and resume firing before waking up from REM sleep (Watson et al., 2010). In addition, the highest firing rate of orexinergic neurons in the lateral hypothalamus is observed during alert and active waking, and lower firing rate is observed during quiet waking, NREM sleep and REM sleep (Mileykovskiy et al., 2005).

Function of sleep

Accumulating evidence support the causal roles of both NREM sleep (Chauvette et al., 2012; Miyamoto et al., 2016; Norimoto et al., 2018; Rasch et al., 2007; Roux et al., 2017; Yang et al., 2014) and REM sleep (Boyce et al., 2016; Dumoulin Bridi et al., 2015; Li et al., 2017) in memory consolidation and synaptic plasticity. In addition, biological changes that occur during NREM sleep support critical roles of this sleep stage in basic functions related to brain maintenance or metabolisms, such as an increase in growth hormone secretion (Gronfier et al., 1996; Takahashi et al., 1968), suppression of cortisol secretion (Gronfier et al., 1997), and activation of the glymphatic system (Xie et al., 2013a). All of these events that accompany NREM sleep likely contribute to the regenerative function of sleep. By contrast, much less is known about how REM sleep might contribute to such basic vital functions, and thus, the function of REM sleep remains poorly understood.

Introduction of cerebral blood flow

Cerebral blood flow (CBF) is critical in maintaining energy-dependent processes, eliminating metabolic byproducts generated by neural activity, and predicting neurotransmitter activities (Dukart et al., 2018). Impaired CBF regulation can affect proteins and ATP synthesis, disrupt generation of action potential, or cause ischemic neuronal death

(Hossmann, 1994). CBF dysregulation is associated with neurodegenerative disorders such as Alzheimer's disease (Kisler et al., 2017). CBF can be affected by numerous factors including the autonomic nervous system, blood pressure, blood viscosity, nitric oxide, carbon dioxide, oxygen by-products from metabolisms and neurotransmitters and so on (Cipolla, 2009; Fantini et al., 2016). Generally, the brain is able to maintain relatively constant CBF within a certain range of systemic blood pressure (Paulson et al., 1990). Therefore, CBF is strictly and independently regulated from the peripheral circulation.

Till now, various approaches have been taken to investigate CBF dynamics across sleep/wake cycles, including positron emission tomography (PET), ultrasound doppler methods, near infrared spectroscopy (NIRS), and functional magnetic resonance imaging (fMRI). However, conflicting conclusions have been drawn from different approaches. According to studies using $H_2{}^{15}O$-PET or NIRS, CBF is decreased during NREM sleep and either comparable to or slightly lower than the awake level during REM sleep (Braun et al., 1997; Kubota et al., 2011). By contrast, according to studies using ultrasonic doppler methods, CBF is highest during REM sleep (Bergel et al., 2018; Grant et al., 2005). In case of fMRI studies, blood oxygen level dependent (BOLD) signals, which correlate with increase in blood flow, during REM sleep have not yet been strictly compared to other stages, whereas during NREM sleep, it becomes higher as sleep becomes deeper compared to the awake state (McAvoy et al., 2018). These conflicts are likely due to differences in the data processing and normalization procedures as well as differences in the type of blood vessels that were observed. In addition, some of the above methods measure a combined effect of CBF and metabolic rates, which makes interpretations even more difficult, as the cerebral metabolic rate also changes along the sleep/wake cycle, with comparable levels between wakefulness and REM sleep and lower levels during NREM sleep, as revealed by ^{18}F-fluoro-2-deoxy-D-glucose PET studies (Maquet et al., 1990).

SPECIFIC AIM

The function of REM sleep is still a large mystery. So far, researches related to REM sleep mostly focus on neuronal functions, such as neuronal activity, synaptic plasticity and so on. In this research, I aim to elucidate the function of REM sleep by focusing on the brain circulatory system.

So far, many approaches were used to analyze the CBF dynamic across wakefulness and sleep, however, conflict results were shown. These conflicts are likely to come from differences in the data processing and normalization procedures as well as from differences in the type of blood vessels that are observed. I realized that current techniques all cannot directly measure blood flow in individual capillaries, where the actual substances exchange between blood and neuron/glia occurs. Therefore, I aim to develop an alternative approach using two-photon microscopy (2PM) to directly measure the movement of individual red blood cells (RBCs) within capillaries across wake/sleep cycle. The results acquired from this new approach should provide a final conclusion on how CBF changes during sleep, and provide critical evidence on how REM sleep contributes to maintaining our health.

MATERIAL AND METHOD

Experimental animals

All animal experiments were approved by the Institutional Animal Care and Use Committee of the University of Tsukuba. Mice were maintained under a 12-h light/dark cycle. Food and water were available *ad libitum*. Strains used in this study were C57BL/6J and *adenosine A_{2A} receptor* knockout ($A_{2A}R$-KO) mice (Chen et al., 1999) in a C57BL/6J background.

Animal surgery for *in vivo* chronic two-photon imaging

Chronic cranial windows were made according to a previous report (Holtmaat et al., 2009). Briefly, adult mice (2-3 months old) were anesthetized with isoflurane (3-5% for induction and 2-2.5% for maintenance) and placed in a stereotaxic frame (David Kopf Instruments). The core body temperature was maintained at 32 to 35ºC using a heating pad. The skull (~3 mm in diameter) over the parietal cortex (1.8 mm lateral and 1.8 mm caudal to bregma) was carefully thinned circularly by a dental drill (Emil Lange C1-500-104-001-001-005, 0.5 mm) and removed using an angle-tipped needle and sharp forceps. A 4 mm-diameter glass coverslip was placed on the dura and sealed with high viscosity type of cyanoacrylate glue (Konishi Co., Ltd. #30523). Two EEG electrodes, which were stainless steel screws, were implanted epidurally over the cortex (1.5 mm lateral and 1.0 mm rostral to lambda, on the hemisphere contralateral to the craniotomy) and the cerebellum (6.8 mm caudal to bregma), respectively. EMG electrodes were stainless steel Teflon-coated wires placed bilaterally into the nuchal muscles and fixed with soldered (Taiyo Electric Ind. Co., Ltd; SE-OST16) ends. Finally, a rectangular aluminum head plate was placed on the skull and attached with dental cement (Super-Bond C&B set; Sun Medical).

In vivo two-photon microscopy

The procedures for in vivo 2PM during sleep/wake states was described previously (Nagayama et al., 2019). Starting from one week after surgery, adult mice (3-5 months old) of either gender underwent a habituation procedure 3 hours a day for at least 7 days to facilitate entrance to sleep in the imaging apparatus. During the habituation and the experiments, mice either stood or sat on an air-floated spherical treadmill while the head was immobilized by clamping the head plate. Capillary CBF was observed using an upright two-photon microscope (Axio Examiner Z1 and LSM 780 NLO, Zeiss) operated by ZEN software

(Zeiss). Fluorescence was excited at 800 nm using a tunable Ti:Sa laser (Maitai DeepSee, Spectra-Physics). Laser were scanned by galvonometric scanners and was focused on the cortical capillaries within 30-50 μm of depth from the brain surface through a 20X water-immersion objective lens (W Plan-Apochromat 20x/NA=1.0, Zeiss). The emitted fluorescence in a range of 500-550 nm from FITC-Dextran was detected with a non-descanned GaAsP detector (BiG, Zeiss).

Capillary CBF was observed between Zeitgeber time (ZT)3 and ZT10, and white noise (70 dB) was applied. Before setting mice to the two-photon microscope, to label the blood plasma, mice received intravenous injection via lateral tail veins of FITC-Dextran with 70 kDa molecular weight (Thermo Fisher Scientific, D1823) at a dose of 5 mg per kilogram body weight in saline. Blood vessels with diameters of 5 μm or less and only single red blood cell (RBC) passing through each point simultaneously were considered as capillaries. Immediately after setting mice on the imaging apparatus, mice typically stayed completely awake and often ran actively on the treadmill for about 2 hours. EEG/EMG recording started during this period, during which data for active wakefulness was collected. For each capillary, repetitive single-line scans were conducted typically along a 20-50 μm range for 500 times with 1.3 milliseconds intervals per line to record the velocity and flow of RBC in XT line scans. Later, when mice entered NREM or REM sleep, XT line scans were performed for the same capillaries. For NREM sleep episodes, the scanning started at least one minute after the transition to NREM sleep. For REM sleep episodes, the first scan started immediately following the transition to REM sleep, but the scans taken during the first 30 seconds of the REM sleep episodes were excluded from the statistical analysis. For each capillary, XT line scans were taken in each sleep/wake state typically 5 to 10 times (minimum 5 times), and each scan was separated by an interval of at least 12 seconds. More frequent scanning was avoided to minimize any deleterious effects of the laser on blood flow. Cerebral cortical areas were determined by referring to the Allan Brain Atlas (http://portal.brain-map.org/). To analyze the changes in the diameter of the capillaries, XT line scans were taken on the transversal direction of the vessel. During subsequent offline analyses, the vigilance states were confirmed based on the EEG/EMG data. Heart rate during REM sleep was measured by counting the number of heart beat spikes recorded in the EMG signal.

EEG/EMG recording under 2PM

To monitor the sleep in mice during 2PM experiment, the EEG and EMG signals were recorded. The EEG and EMG signals were amplified 40,000x and 4,000x respectively and filtered with a pass-band of 0.5-500 Hz for the EEG signals and 1.5-1000 Hz for the EMG signals by an analog amplifier (MEG-5200, NIHON KOHDEN). The EEG/EMG signals were then digitized at a sampling rate of 2000 Hz by a 16-bit analog-to-digital converter (Digidata 1440A, Molecular Devices), and collected by Clampex 10.3 software (Molecular Devices). The scan signals for 2PM were also digitized and recorded by the same systems to temporally match the scan timing with the EEG/EMG data.

Sleep stages analysis

EEG signals were subjected to fast Fourier transform and further analysis using a custom-written MATLAB-based algorithm. The vigilance state was classified as REM sleep, NREM sleep, or wake based on absolute delta (δ; 0.5-4 Hz) power, theta (θ; 6-10 Hz) power to δ power ratio, and the integral of EMG signals. We applied 10-s sliding window epochs. Epochs with high EMG and low δ power were classified as wake. Epochs with high δ power and low EMG were classified as NREM sleep. Epochs with high θ/δ ratio and extremely low EMG were classified as REM sleep.

Analysis of XT line scan images

XT line scan images were binarized to allow detection of individual RBC. Then, for each binarized image, the RBC velocity (distance/time) and flow (1 RBC/time) were calculated by measuring the average slope and number of lines, respectively, using custom-written MATLAB-based algorithms. For each capillary, the mean value was calculated from multiple (at least 5) scan images for each vigilance state. The experimenter was blinded to sleep stages when analyzing all line scan images.

Flowerpot method of REM sleep disturbance

The flowerpot method was performed following a previous paper (Verret et al., 2006). Briefly, a stainless-steel platform (3 cm in diameter and height) was placed in a cage that was filled with water to the depth of 2 cm. Food and water were easily accessible to the mice from the top. Mice were applied to this cage for 23.5 hours starting from ZT4.5. Then, mice were given a 30-minute rest period in the home cage, during which the flowerpot cage was

cleaned. This was repeated for 2 days (for simultaneous 2PM imaging and EEG/EMG recording) or 3 days (for EEG/EMG recording only). Similar to other experiments, 2PM imaging was performed from ZT5 to ZT8, considering that the REM sleep rebound was very high during this period (**Fig. 4a**).

$NaHCO_3$ and $A_{2A}R$ PAM-1 administration

$NaHCO_3$ (Wako-Fujifilm, 199-01351) was dissolved in distilled water (1M) and administered intraperitoneally (1.7 g per kilogram weight). Adenosine A_{2A} receptor positive allosteric modulator ($A_{2A}R$ PAM-1) was prepared following a previous paper (Korkutata et al., 2019) and was dissolved in saline (7.5 mg/ml) and administered intraperitoneally (75 mg per kilogram weight).

EEG/EMG recording from freely moving mice

To confirm the occurrence of a REM sleep rebound following the flowerpot method and to compare the EEG power spectrum between *$A_{2A}R$* -WT and *$A_{2A}R$*-KO mice, EEG/EMG signals were obtained from freely moving mice following a previous study (Hayashi et al., 2015). Briefly, EEG electrodes were implanted epidurally over the parietal cortex and cerebellum and EMG electrodes were placed bilaterally into the trapezius muscles, similar to the mice used in 2PM imaging experiments. The mice were allowed to recover in their home cage for at least 3 weeks and then habituated to the sleep recording cages for 5 days. The EEG/EMG data were filtered (band pass 0.5-250 Hz) and collected and digitized at a sampling rate of 500 Hz, and further filtered post hoc by software (EEG: high pass 0.5 Hz). For judging vigilance stages, EEG signals were subjected to fast Fourier transform and further analysis using SleepSign (Kissei Comtec, Nagano, Japan). The vigilance state in each 4-s epoch was manually classified as wakefulness, NREM sleep, or REM sleep based on the same criteria used in 2PM imaging. If a single epoch contained multiple states, the state with the longest duration was assigned. For EEG power spectrum comparison, a custom-written MATLAB-based algorithm was used. For each individual, the average EEG power spectrum of wakefulness, NREM sleep and REM sleep epochs was calculated and normalized by the total EEG power across all frequencies and across all 24 h. To avoid the effect of mixed states, any epochs which contained multiple states were excluded.

Statistics

All statistical analyses were performed in Prism8 (GraphPad). All values represent the mean of all samples in each group with mean ± s.e.m., except for Figure 5. The number of capillaries scanned per mouse was depending on the number of REM sleep episodes engaged in individual animals during 2PM imaging. In general, at least 2 capillaries per mouse were analyzed in all figures, except for one wild-type and two $A_{2A}R$-KO mice from which only 1 capillary was taken into statistical analysis. Detailed sample sizes, gender distributions, statistical methods and results of each group are indicated within each figure.

RESULTS

1. Capillary CBF analysis in an unanesthetized mice across wake/sleep cycle

1-1. Development of using two-photon microscopy to directly measuring the capillary CBF

To analyze how CBF is regulated across wake/sleep cycle, I developed an alternative approach to directly measure the velocity and number of an individual red blood cell (RBC) within capillaries by means of two-photon microscopy **(Fig. 1a)**. Capillaries in cortex layer I, typically between 30 to 50 μm from the brain surface, were targeted for observation **(Fig. 1b)**, and sleep stages were simultaneously monitored by recording EEG and EMG **(Fig. 2a)**. Capillaries in deeper areas were avoided since fluorescent signals derived from the dye faded by the time the animal started to engage in REM sleep (approximately 3 hours after injecting the dye). Distance (X)- Time (T) line scans acquired in the longitudinal direction of the capillary allowed to record the temporal change in the positions and numbers of individual RBCs **(Fig. 1b, c and 2b-e)**. Therefore, the RBC velocity (μm/ms) and RBC flow (defined as the number of RBC passing through a defined point; 1RBC/ms) can be calculated from XT line scans taken at a specific sleep stage.

2. The role of sleep in cerebral capillary blood flow regulation

2-1. Capillary CBF upsurged during REM sleep, but showed no significant difference between wakefulness and NREM sleep

According to the location of the optical window created, primary somatosensory cortex, secondary visual cortex and parietal cortex which include both primary and secondary cortices were analyzed in my study. As a result, all cortical areas exhibited significant elevated capillary CBF during REM sleep in terms of both RBC velocity and RBC flow compared to the other stages **(Fig. 3a-c)**. By contrast, there were no significant differences between active wakefulness and NREM sleep in RBC velocity or flow. In addition, I did not detect a significant difference in capillary diameters change across awake and sleep states **(Fig. 3d)**, which suggested that the elevated capillary CBF during REM sleep is likely not

due to the diameter of individual capillaries but rather than some changes in the pre-capillary arteries or further upstream structures.

2-2. Larger elevation in capillary RBC flow during the rebound REM sleep observed after REM sleep disturbance.

To investigate whether capillary CBF during REM sleep is affected by preceding homeostatic REM sleep pressure. I applied the flower pot method on mice before CBF imaging to disturbs sleep, especially REM sleep, and thus leads to a strong REM sleep rebound (Maloney et al., 1999; Verret et al., 2006). I confirmed that REM sleep is largely increased for hours after applying the flower pot method to mice **(Fig. 4a).** During the rebound REM sleep, capillary CBF elevation was significantly enhanced compared to basal REM sleep in terms of increased RBC flow, and, although not significant, a tendency for an increase in the RBC velocity was observed **(Fig. 4b, c)**, suggesting that the system underlying the increased capillary CBF during REM sleep is at least partly under control of REM sleep pressure.

2-3. Capillary CBF slowly rose after entering REM sleep and slowly declined after waking up from REM sleep

While analyzing capillary CBF across sleep/wake in mice, I observed that, upon entering REM sleep, capillary CBF in term of both RBC velocity and flow gradually increased across a period of approximately 30 to 50 seconds and was kept at a high level thereafter with some fluctuation until REM sleep termination, after which it gradually decreased **(Fig. 5a-f)**. Thus, in contrast to rapid changes in the EEG **(Fig. 5a,b)** and EMG during transitions into or out of REM sleep, capillary blood flow might be regulated by some slow mechanisms (for example, secretory factors that are slowly up-regulated during REM sleep and then acting to dilate or contract blood vessels).

3. Sleep architecture in adenosine A_{2A} receptor knockout mice

3-1. 24-hour of sleep recording in *$A_{2A}R$*-WT and *$A_{2A}R$*-KO mice

The results so far indicated that capillary CBF is largely elevated during REM sleep, which might be mediated by some secretory factors up- or down-regulated in REM sleep. As an entry point addressing the mechanism of REM sleep in enhancing capillary CBF, I next

focused on adenosine. Adenosine is known to be released by neurons and glia and acts as a vasodilator via the adenosine A_{2A} receptor (A_{2A}R) (Ngai et al., 2001). In addition, A_{2A}R is a target of caffeine in sleep inhibition, supporting its involvement in sleep regulation, although *A_{2A}R* knockout (*A_{2A}R*-KO) mice do not exhibit advert sleep abnormality nor cardiovascular deficits at baseline (Chen et al., 1999; Huang et al., 2005).

I firstly performed sleep recording on freely moving animals to examine whether A_{2A}R deficiency would drastically change the sleep architecture. In my results, total time spent in wakefulness, NREM sleep and REM sleep showed no significant difference between *A_{2A}R*-WT and *A_{2A}R*-KO mice (**Fig. 6a, g-i**). When I separately compared the light and dark phases, time spent in REM sleep was significantly increased during the light phase in *A_{2A}R*-KO mice (**Fig. 6d**). The duration and number of episodes were not significantly altered in *A_{2A}R*-KO mice during wakefulness (**Fig. 6b,c,e,f**), while the episode duration of both NREM and REM sleep was reduced (**Fig. 6b**). Furthermore, the episode number of REM sleep increased mainly during the light phase (**Fig. 6c,f**).

3-2. EEG power density in *A_{2A}R*-KO mice was lower during NREM sleep in the delta range, but overall higher during REM sleep

To access EEG activity in mice with and without A_{2A}R, I compared the normalized EEG power spectrum of wakefulness, NREM sleep and REM sleep between *A_{2A}R*-WT and *A_{2A}R*-KO mice across 24 hours or during the light and dark phases. In *A_{2A}R*-KO mice, the EEG power density was decreased in the delta range (1.5-2.5 Hz) during NREM sleep, while the EEG power density was increased during REM sleep across 24 hours or the light and dark phases (**Fig. 7b,c**). During wakefulness, there was no significant difference between the genotypes across 24 hours or the dark phase, however, there was a significant genotype effect on the EEG power density during the light phase (**Fig. 7a**). In summary, congenital lack of A_{2A}R has no large change, but minor disruption, on the basal sleep structure in mice.

4. The involvement of adenosine A_{2A} receptor in CBF regulation during sleep

4-1. Adenosine A_{2A} receptor knockout mice exhibited an impairment in the upsurge of CBF during REM sleep

After I established that there is no drastic change in the sleep architecture of *A_{2A}R*-KO mice, I started to examine the role of A_{2A}R in CBF regulation during sleep by analyzing the

capillary CBF across sleep/wake cycle in *$A_{2A}R$*-KO mice. In my results, capillary CBF in *$A_{2A}R$*-KO mice was elevated during REM sleep in terms of both RBC velocity and flow, but to a much lesser extent compared to wildtype mice in terms of RBC velocity **(Fig. 8a, b)**. No significant decrease in CBF was detected during active wakefulness nor NREM sleep state **(Fig. 8b)**. The selective effect of *$A_{2A}R$*-KO on capillary CBF during REM sleep was further supported by a significant decrease in the ratio of capillary CBF during REM sleep over NREM sleep, but not wakefulness over NREM sleep **(Fig. 8c,d)**. There was also a significant decrease in the ratio of capillary RBC velocity but not RBC flow during REM sleep over wakefulness in *$A_{2A}R$*-KO **(Fig. 8e).**

4-2. Similar capillary CBF responses to sodium bicarbonate in WT and *$A_{2A}R$*-KO mice

To examine whether the reduction of CBF observed in *$A_{2A}R$*-KO mice was due to the impaired vascular function or was indeed due to the lack of $A_{2A}R$, the vascular response to sodium bicarbonate ($NaHCO_3$), a reagent that increases CBF (Buckley et al., 2013; Yoon et al., 2012), were tested in wild-type (WT) and *$A_{2A}R$*-KO mice. From my results, both WT and *$A_{2A}R$*-KO mice increased RBC flow but not RBC velocity after $NaHCO_3$ treatment, which suggested that the general responsiveness of vasculature in *$A_{2A}R$*-KO mice was likely unchanged as suggested by the comparable responses between WT and *$A_{2A}R$*-KO mice to $NaHCO_3$ **(Fig. 9a, b)**.

4-3. Elevation of RBC velocity across the sleep/wake cycle in response to $A_{2A}R$ positive allosteric modulator in WT mice

To elucidate whether adenosine acts locally or whether the systemic action of adenosine at another site is important in regulating CBF during REM sleep, pharmacological experiment was conducted by using $A_{2A}R$ positive allosteric modulator ($A_{2A}R$ PAM-1) (Korkutata et al., 2019). Increased RBC velocity, but not RBC flow was observed in all stages after treating WT mice with $A_{2A}R$ PAM-1 **(Fig. 10a)**, while no significant difference were detected in the ratio of capillary CBF during REM sleep over NREM sleep or active wakefulness, nor active wakefulness over NREM sleep **(Fig. 10b-d)**.

4-4. Comparison of various measures of REM sleep (heart rate, episode duration, EEG power spectrum) between WT and *$A_{2A}R$*-KO mice

To access other possible causes of lower CBF during REM sleep observed in $A_{2A}R$-KO mice, I also compared the heart rate, the episode duration of REM sleep, as well as the EEG power spectrum between WT and $A_{2A}R$-KO mice.

In the current results showed in the CBF study, only the REM sleep episodes with durations longer than 40 seconds were analyzed since CBF gradually elevates after entering REM sleep (**Fig. 5a-f**). Thus, the heart rates and the average episode duration were obtained from the REM sleep episodes that underwent CBF analyses, and EEG power spectra were obtained by EEG/EMG recording from freely moving mice where episodes lasting 40 seconds or longer were extracted. As a result, the heart rate calculated from the spikes recorded in the EMG signal during REM sleep between WT and $A_{2A}R$-KO mice showed no significant difference **(Fig. 11a)**. There was also no significant difference in the duration of REM sleep episodes analyzed in this CBF study between WT and $A_{2A}R$-KO mice **(Fig. 11b)**. Furthermore, the EEG power density of REM sleep was significantly higher in $A_{2A}R$-KO mice than $A_{2A}R$-WT mice, especially around the theta range, suggesting that REM sleep is not overall deteriorated. **(Fig. 11c)**.

DISCUSSION

CBF dynamics across sleep/wake cycle in wild type mice

By observing the movements of individual RBC in cerebral capillaries, I achieved direct measurements of capillary CBF changes across the sleep/wake cycle. Capillary CBF was drastically increased during REM sleep in all three cortical areas that I analyzed. This finding does not match with studies that applied $H_2{}^{15}O$-PET in humans to conclude that CBF is highest during wakefulness in many cortical areas (Braun et al., 1997), whereas it is consistent with a study that applied an ultrasound imaging technique in rats to conclude that blood flow is increased during REM sleep in multiple brain areas (Bergel et al., 2018). These differences are likely attributed to the data processing and normalization procedures as well as the type of blood vessels that were observed, although differences in animal species might also be involved. The advantage of my method was that it is subjected to minimal normalization procedures and that it detected blood flow from capillaries, where the actual substance exchange occurs. I also demonstrated that capillary CBF appeared the same between active wakefulness and NREM sleep, which is inconsistent with studies using $H_2{}^{15}O$-PET (Braun et al., 1997), ultrasound doppler methods (Grant et al., 2005), NIRS (Kubota et al., 2011), or fMRI (McAvoy et al., 2018), and perhaps surprising considering that the average firing rates of pyramidal cells and the metabolic rates are largely decreased during NREM sleep (Evarts, 1964; Maquet et al., 1990). Interestingly, a recent study suggested that the burst firing of pyramidal neurons in the UP state of NREM sleep was higher than that in wakefulness (Watson et al., 2016). It is possible that the average firing rate of pyramidal neurons during NREM sleep is lower than the awake stage considering that NREM sleep shows a large fraction of time window with all neurons silent in its DOWN state, corresponding to alternating with non-silent UP states. The burst firing of neurons in the ON state of NREM sleep may be the reason why CBF is comparable between NREM sleep and wakefulness.

The involvement of adenosine A_{2A} signaling in the CBF increase during REM sleep

During transitions to and from REM sleep, I observed a temporal delay in the changes in capillary CBF relative to the changes in cortical EEG. Thus, although changes in cortical EEG itself should have some effects on CBF via neurovascular coupling, additional mechanisms are likely involved. I demonstrated that the $A_{2A}R$ is crucial for the drastic elevation of capillary CBF during REM sleep, whereas it is dispensable for maintaining

capillary CBF during active wakefulness or NREM sleep. Although increase in heart rate might be one factor contributing to the increased CBF during REM sleep, *$A_{2A}R$*-KO mice exhibited normal heart rates during REM sleep, implicating that the CBF is regulated independently from the peripheral. It is not known whether extracellular levels of adenosine in the cerebrum increase during REM sleep. In addition to CBF, REM sleep enhances slow wave activity (SWA) in the subsequent NREM sleep episode (Hayashi et al., 2015). Considering that SWA is also enhanced by adenosine, via the adenosine 1A receptor (Benington et al., 1995; Bjorness et al., 2009), adenosine signaling might be somehow upregulated during REM sleep. While the average firing rate of pyramidal cells is highest during wakefulness, pyramidal cells tend to fire in bursts during REM sleep (Evarts, 1964), which might contribute to enhanced adenosine signaling. Future imaging studies using recently developed adenosine imaging FRET probes (Hoffmann et al., 2005) may reveal how extracellular adenosine levels change temporally and spatially across sleep/wake.

In addition to adenosine, increased acetylcholine and decreased noradrenaline, 5-HT, orexin and histamine during REM sleep (Monti, 2013) may also contribute to the elevated CBF. Unfortunately, most sleep-state related neurotransmitters or neuromodulators interfere sleep in animals when their antagonists/agonists are systemically administrated, such as atropine (acetylcholine receptor antagonist), reboxetine (noradrenaline uptake inhibitor) and zm241385 ($A_{2A}R$ antagonist) which I have tested and was not successful in obtaining REM sleep for CBF analysis. Therefore, local microinjection of these drugs by inserting a glass capillary into the cerebral cortex through a silicone access port (Roome and Kuhn, 2014) on the cranial window might be an alternative approach to pharmacologically examining the molecular mechanism of CBF regulation during sleep in the future.

Analytical perspective on capillary RBC velocity and RBC flow

The delivery of energy substances and the removal of waste metabolic products at the tissue level are largely mediated by blood perfusion in capillaries. The exchange of substances is executed by the passage of RBCs which compress and flow through capillaries in a single-file manner. Hence, directly analyzing the CBF during sleep at the level of capillary brings a new perspective on the biology of sleep.

The advantage of my approach of using 2PM is that it could detect changes in both capillary RBC velocity and flow. RBC flow is determined by RBC velocity and density, which can be differently regulated under some circumstances (Chaigneau et al., 2003). Although capillaries with high RBC flow generally have high RBC velocity (Kleinfeld et al.,

1998), capillaries with similar RBC velocities may exhibit dramatically different RBC flow. (Guevara-Torres et al., 2016). Notably, my results show that REM sleep pressure enhanced RBC flow but not velocity, suggesting that the density of RBC was selectively upregulated under such condition. $NaHCO_3$ also increased the flow of RBC but not the velocity in both WT and $A_{2A}R$-KO mice. At the tissue level, the number of RBC passages is a more important determinant of capillary perfusion than RBC velocity alone (Lecoq et al., 2011; Parpaleix et al., 2013). However, it is still unclear what the role of RBC velocity is in terms of biological function. In the future, it would be interesting to address the molecular mechanism underlying respective actions of REM sleep on RBC velocity and density.

The size and number of RBC positively correlates with hematocrit (volume ratio of RBCs: total blood). Hence, change in hematocrit might be a possible mechanism responsible for enhanced RBC velocity and flow during REM sleep. Comparing the XT line scans taken during active wakefulness, NREM and REM sleep, the lines in the scans appear to be thinner during REM sleep compared to the other two stages. This phenomenon could result from the decrease in RBC size probably due to erythrocyte deformation (Wei et al., 2016), however, along with the increased RBC number, the hematocrit during REM sleep may not significantly alter. Since I did not measure the hematocrit in the capillaries, it is difficult to know the dynamics of hematocrit across wake/sleep. Future studies may consider to measure the capillary hematocrit (Guevara-Torres et al., 2016) to clarify whether the change in hematocrit occurs in REM sleep.

Systemic blood pressure is unlikely involved in the enhancement of CBF during REM sleep due to the autoregulation of the cerebral blood flow. However, it is possible that elevation of RBC velocity and flow resulted from the neural activation during REM sleep that induces an increase in the local blood pressure upstream or decrease in impedance downstream of the recorded capillaries. The similar functional recruitment of RBCs by neuronal activation has already been reported in cerebellar cortex of rats by scanning laser-Doppler flowmetry (Akgören and Lauritzen, 1999).

On the other hand, blood viscosity is directly correlated with the hemoglobin concentration and hematocrit. According to mathematical equations, low hematocrit decreases blood viscosity and thus increases CBF (Fantini et al., 2016). In contrast, my results show that both RBC density and CBF were upregulated during REM sleep. Hence, it is likely that REM sleep involves other factors such as local blood pressure in regulating CBF.

Sleep architecture in Adenosine A_{2A} receptor knockout mice

Previous study shows that the circadian sleep/wake profile in WT mice but not *$A_{2A}R$*-KO mice is not affected by caffeine (Huang et al., 2005), however, the basal sleep of *$A_{2A}R$*-KO mice remains unclear. In this study, I compared the basal sleep between *$A_{2A}R$*-WT and *$A_{2A}R$*-KO mice. In my results, although total sleep amount of *$A_{2A}R$*-KO mice was comparable to *$A_{2A}R$*-WT mice, *$A_{2A}R$*-KO mice exhibited less REM sleep duration and more bout number compared to *$A_{2A}R$*-WT mice. In the future, it would be interesting to investigate whether the decline of CBF during REM sleep in *$A_{2A}R$*-KO mice fails to maintain the duration of REM sleep and results in generating more REM sleep due to the REM pressure.

Functional significance of CBF elevation during REM sleep

The elevated capillary CBF detected in my study might be important for sufficient exchange of substances between the brain and the blood. Both reduction in REM sleep amount and CBF precede dementia including Alzheimer's disease (Pase et al., 2017; Sweeney et al., 2018). A recent study showed that neutrophil adhesion in capillaries results in CBF reduction in Alzheimer's disease mouse models (Cruz Hernández et al., 2019). The high capillary CBF during REM sleep might act as a flushing force to eliminate the plugged neutrophils and reduce the capillary occlusion. In addition, given that arterial pulse drives the flow of the glymphatic system (Iliff et al., 2013) and the meningeal lymphatics (Louveau et al., 2015), high CBF in REM sleep might contribute to promoting brain waste clearance via activation of the glymphatic system (Xie et al., 2013b) or meningeal lymphatic system (Mesquita et al., 2018) during subsequent NREM sleep. My approach of simultaneous capillary CBF observation combined with EEG/EMG recording is expected to be also effective for future studies that test these possibilities and elucidate the functional significance of the capillary CBF upsurge during REM sleep.

Development and troubleshooting of CBF analysis by two-photon microscopy

Infection or inflammation under cranial window between cortex and glass coverslip generates milky substances ("white window") in the following days after surgery which is irreversible and impenetrable by laser, and it is unable to perform two-photon imaging under this condition. In most cases, this mouse should be discarded as the cranial window is compromised. Therefore, the surgical procedure of cranial window should keep as sterile as possible to prevent any infection occurs. Dura damage or entry of dust (bond dust, dust from

marker pen, metal dust generated during bending the needle, etc.) into the opened cortex should be avoided during surgery to prevent inflammation. However, ethanol should be avoided applying on the sterilization of glass coverslip which is one cause of the white window. On the other hand, bleedings under cranial window in most cases would be absorbed by tissue itself within a couple days and not affecting follow-up imaging.

Habituation of mice upon air-floated spherical treadmill can start one-week after the surgery. Habituation typically held 3 hours per day for 7 days to train the mice becoming familiar to the air-floated treadmill system. Two-photon imaging on blood vessels should be performed at least 2 weeks after surgery to allow stabilization of angiogenesis under cranial window. For longer imaging needs, mice should be trained minimally once in every 2 weeks or re-performing the 7-day habituation before the next imaging section.

CONCLUSION

For the first time, capillary RBC velocity and flow were directly analyzed in unanaesthetized mice during sleep/wake cycle by two-photon microscopy in this study. Through this approach, I identified a novel pattern of CBF across sleep/wake cycle and succeeded in drawing a final conclusion. I show that CBF is greatly elevated during REM sleep, while, surprisingly, the CBF is comparable between wakefulness and non-REM sleep. This is largely different from how the firing rate of cortical neurons changes across sleep/wake stages. Moreover, I identified that adenosine A_{2A} receptor is critical for the regulation of CBF specifically during REM sleep, but not required for CBF regulation in other sleep/wake stages. The approach of simultaneous capillary CBF observation combined with EEG/EMG recording is expected to be also effective for future studies that test these possibilities and elucidate the functional significance of the capillary CBF upsurge during REM sleep.

FIGURES

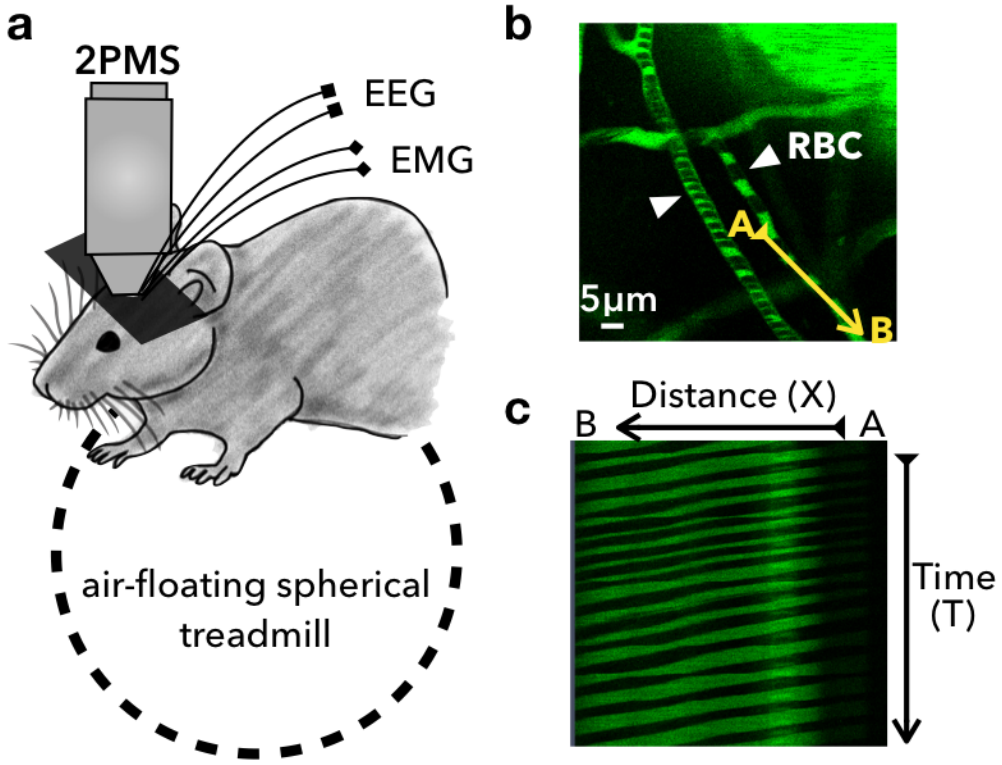

Figure 1. Experimental method for measuring capillary CBF across sleep/wake in mice. **a**, Schematic illustration of the setup for simultaneous 2PM imaging and EEG/EMG recording in mice. Mice were trained to be able to sleep on an air-floating spherical treadmill with head fixed by a head plate in advance, and imaging was performed through an opened cranial window. **b**,**c**, Representative images of cortical vasculature visualized by labeling blood plasma with FITC-Dextran (green). Note that RBC are not labeled and thus appear black (arrow heads). Movements of RBC were recorded by repetitive single-line scans taken on the longitudinal direction along the capillary from point A to B (yellow line). **c**, Line scans obtained in **b** were used to generate a distance-time line scan (XT line scan) image. From the XT line scan image, RBC velocity and RBC flow were calculated.

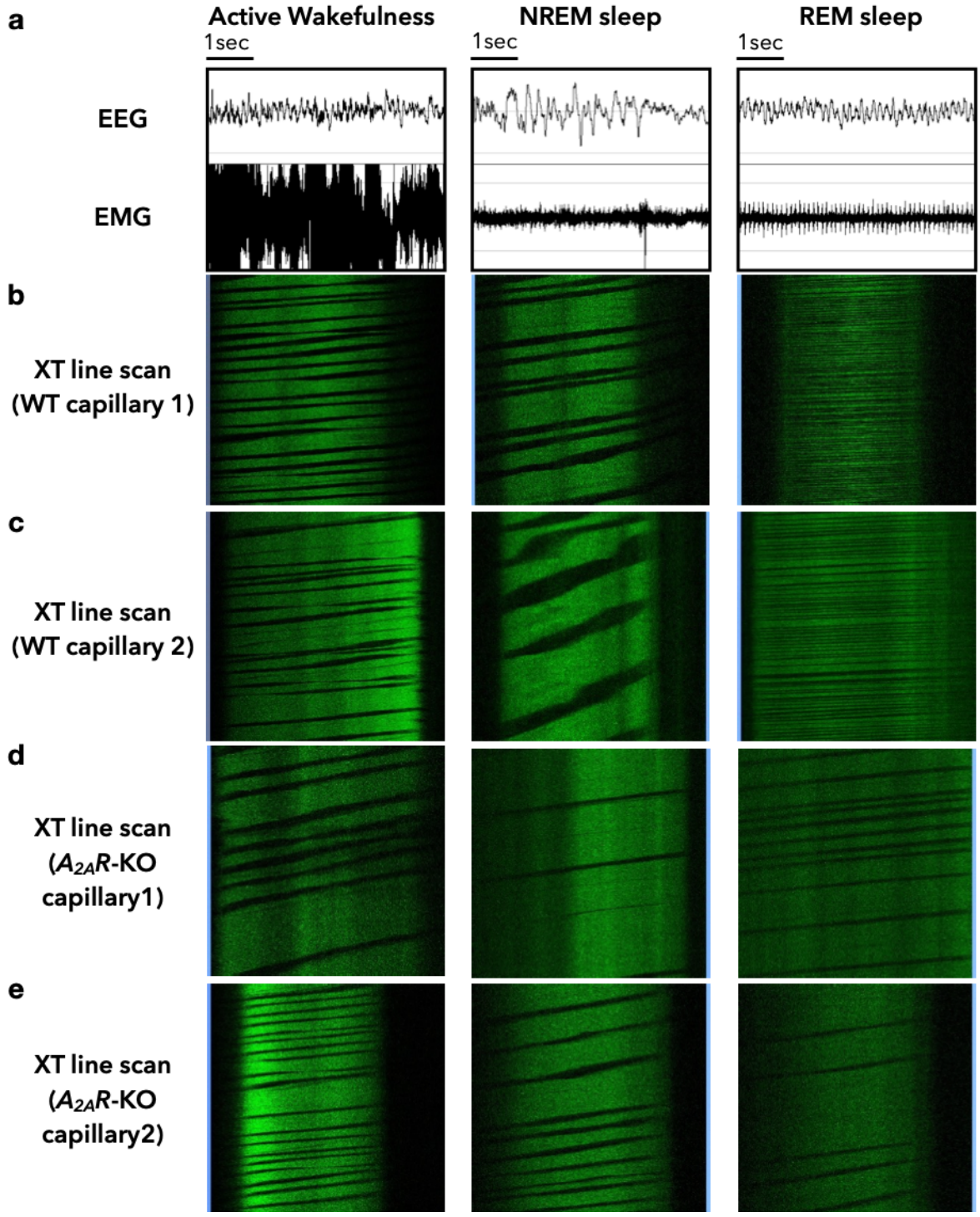

Figure 2. Representative images of EEG/EMG signals and XT line scans.

a, Representative images of EEG and EMG signals during active wakefulness, NREM sleep and REM sleep. **b-e**, Representative XT line scan images taken from cerebral capillaries in WT **(b,c)** and $A_{2A}R$-KO **(d,e)** mice during active wakefulness, NREM sleep and REM sleep. Each scan lasted 650 milliseconds.

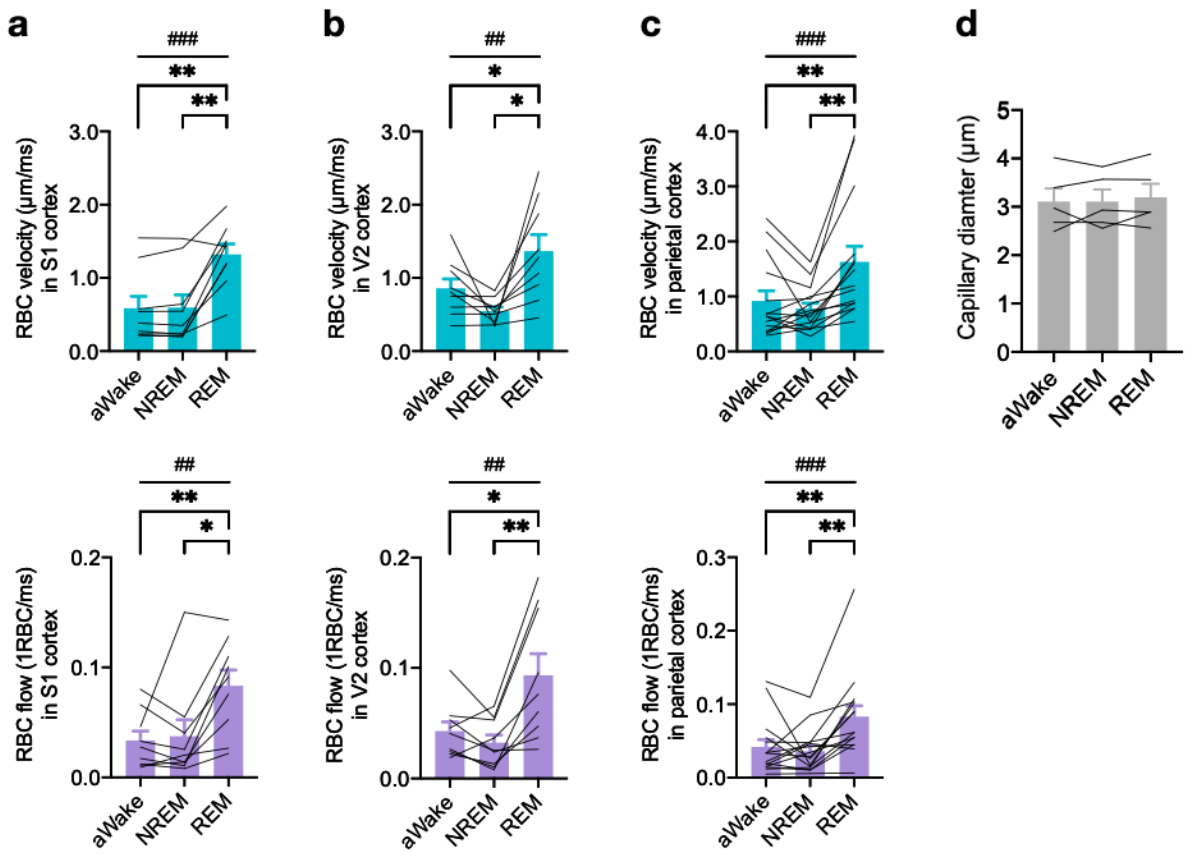

Figure 3. Capillary CBF is largely elevated during REM sleep, whereas is comparable between wakefulness and NREM sleep.

a-c, RBC velocity and flow (mean± s.e.m.) during active wakefulness (aWake), NREM sleep (NREM) and REM sleep (REM) in the primary somatosensory (S1) cortex (**a**; n= 9 capillaries; 3 mice (1 female, 2 males)), secondary visual (V2) cortex (**b**; n= 9 capillaries; 3 mice (1 female, 2 males)), and parietal cortex (**c**; n= 15 capillaries; 6 mice (2 females, 4 males)). # indicates significant effect of sleep/wake state in repeated-measures one-way ANOVA (## P<0.01; ### P<0.001). * indicates significance in the post-hoc Tukey's multiple comparisons test (* P <0.05; ** P <0.01). **d**, Changes in the diameter of capillaries (mean± s.e.m.) across sleep/wake cycles (n= 5 capillaries; 3 mice (2 females, 1 male)). No significant effect of sleep/wake state was detected in the repeated-measures one-way ANOVA. Each line represents an individual capillary.

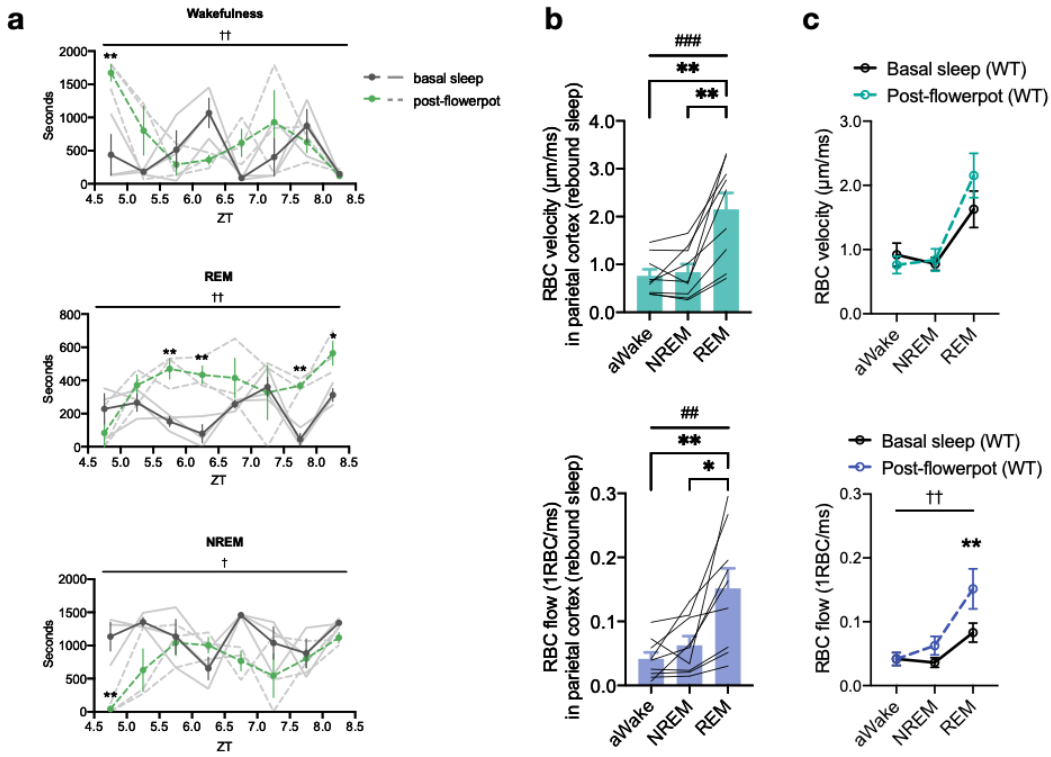

Figure 4. Larger elevation in capillary RBC flow during the rebound REM sleep observed after flowerpot method of sleep disturbance.

a. Time spent (mean± s.e.m.) in wakefulness **(a)**, REM sleep **(b)** and NREM sleep **(c)** under basal condition (basal sleep, grey line) and immediately after application to the flowerpot (post-flowerpot, green dashed line) in $A_{2A}R$-WT mice (n=3 male mice). Application to the flowerpot ended at Zeitgeber time (ZT)4. Each dot represents the time spent in each stage every 30 minutes. † indicates a significant interaction between conditions and ZT in repeated-measures two-way ANOVA († P <0.05; †† P <0.01). * indicates significance in post-hoc Sidak's multiple comparisons test at each time point (* P <0.05; ** P <0.01). **b.** RBC velocity and flow (mean± s.e.m.) in the parietal cortex immediately after subjecting mice to 2 days of flowerpot method of sleep disturbance (n= 9 capillaries; 3 mice (1 female, 2 males)). # indicates significant effect of sleep/wake state in repeated-measures one-way ANOVA (## P<0.01; ### P<0.001). * indicates significance in the post-hoc Tukey's multiple comparisons test (* P <0.05; ** P <0.01). Each line represents an individual capillary. **c**, Comparison of RBC velocity and flow (mean± s.e.m.) between natural sleep and sleep after 2 days of flowerpot method in the parietal cortex across sleep/wake cycles (same data shown in **3c** and **4b**). † indicates significant interaction between the condition and sleep/wake state in repeated-measures two-way ANOVA (†† P <0.01). * indicates significance in the post-hoc Sidak's multiple comparisons test (** P <0.01). Each line represents an individual capillary.

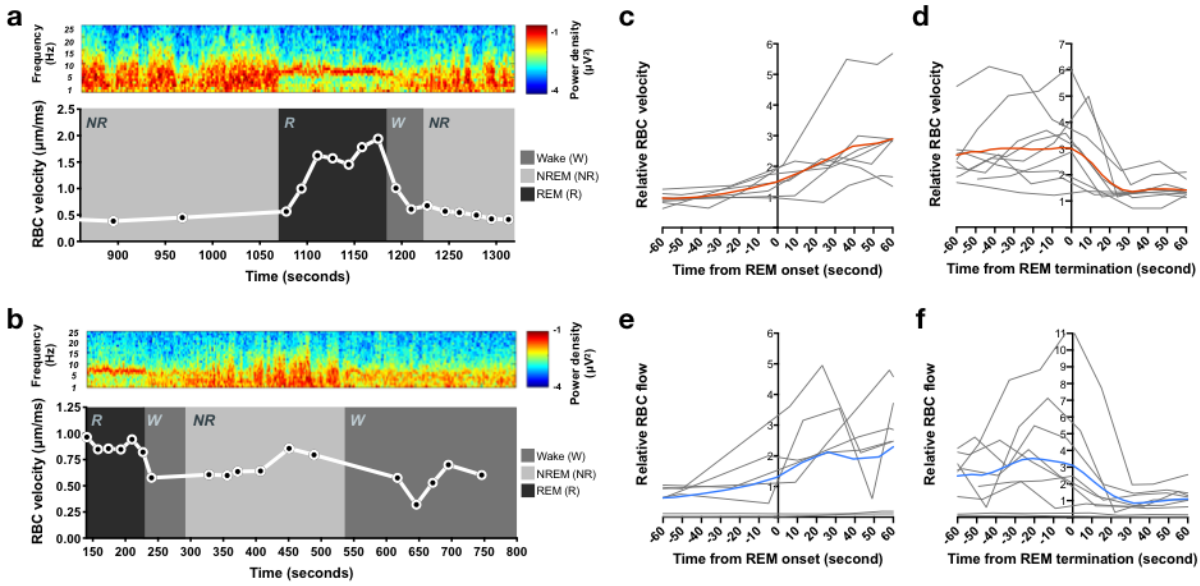

Figure 5. Temporal dynamics of capillary CBF across sleep/wake cycle.

a, b, Representative datum showing temporal changes in the EEG power spectrum and the RBC speed of a capillary during a period containing episodes of NREM sleep (NR), REM sleep (R) and sustained active wakefulness (W). Note that the wakefulness episode is longer in the recording in **b** than in **a**. The animal entered an active wakefulness state after NREM sleep in **b**, where it ran actively on the treadmill. **c-f,** Temporal changes in relative RBC velocity (**c,d**) and flow (**e,f**) around transitions from NREM sleep to REM sleep (**c,e**) and REM sleep to wakefulness (**d,f**). Of the capillaries analyzed in **3a-c**, those whose measurements around the timing of state transitions were available were plotted. In **c-f**, each grey line represents an individual capillary, and the red and blue line represents the mean value of RBC velocity and flow respectively.

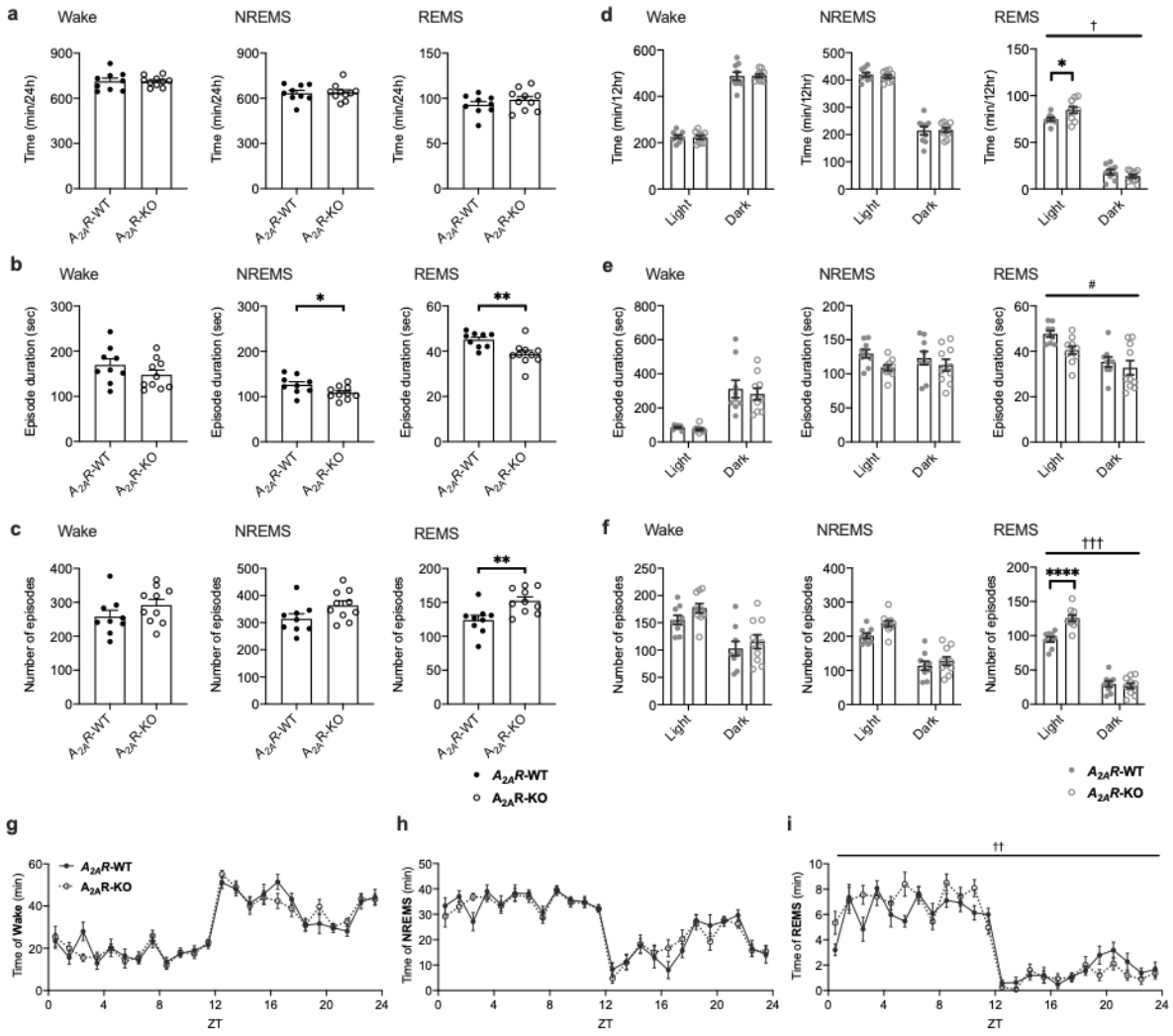

Figure 6. 24-hour of sleep recording in *A2AR*-WT and *A2AR*-KO mice on the 3rd week after surgery.

a-c, Total amount (**a**), episode duration (**b**), and episode number (**c**) of wakefulness, NREM sleep and REM sleep in *A2AR*-WT (closed circle) and *A2AR*-KO (open circle) mice during 24 hours are shown (n= 9 male *A2AR*-WT mice, n=10 male *A2AR*-KO mice). * indicates significance in Welch's test (* $P < 0.05$; ** $P < 0.01$). **d-f**, total amount (**d**), episode duration (**e**), and episode number (**f**) of wakefulness, NREM sleep and REM sleep in *A2AR*-WT (closed circle) and *A2AR*-KO (open circle) mice during the light and dark phases. # and † indicate significant main effect of genotype and significant interaction between genotype and light/dark phase, respectively, in two-way repeated-measures of ANOVA (#, † $P < 0.05$; ††† $P < 0.001$). Each closed/open circle represents an individual mouse. All bar graphs represent the mean of all samples in each group with mean ± s.e.m. * indicates significance in post hoc Bonferroni's multiple comparison test (* $P < 0.05$; **** $P < 0.0001$). (**g-i**) Daily variations in the amount of wakefulness (**g**), NREM sleep (**h**) and REM sleep (**i**) every hour in *A2AR*-WT (closed circle, solid line) and *A2AR*-KO (open circle, dotted line) mice. † indicates significant

interaction between genotype and ZT in two-way repeated-measures of ANOVA (†† $P <$ 0.01).

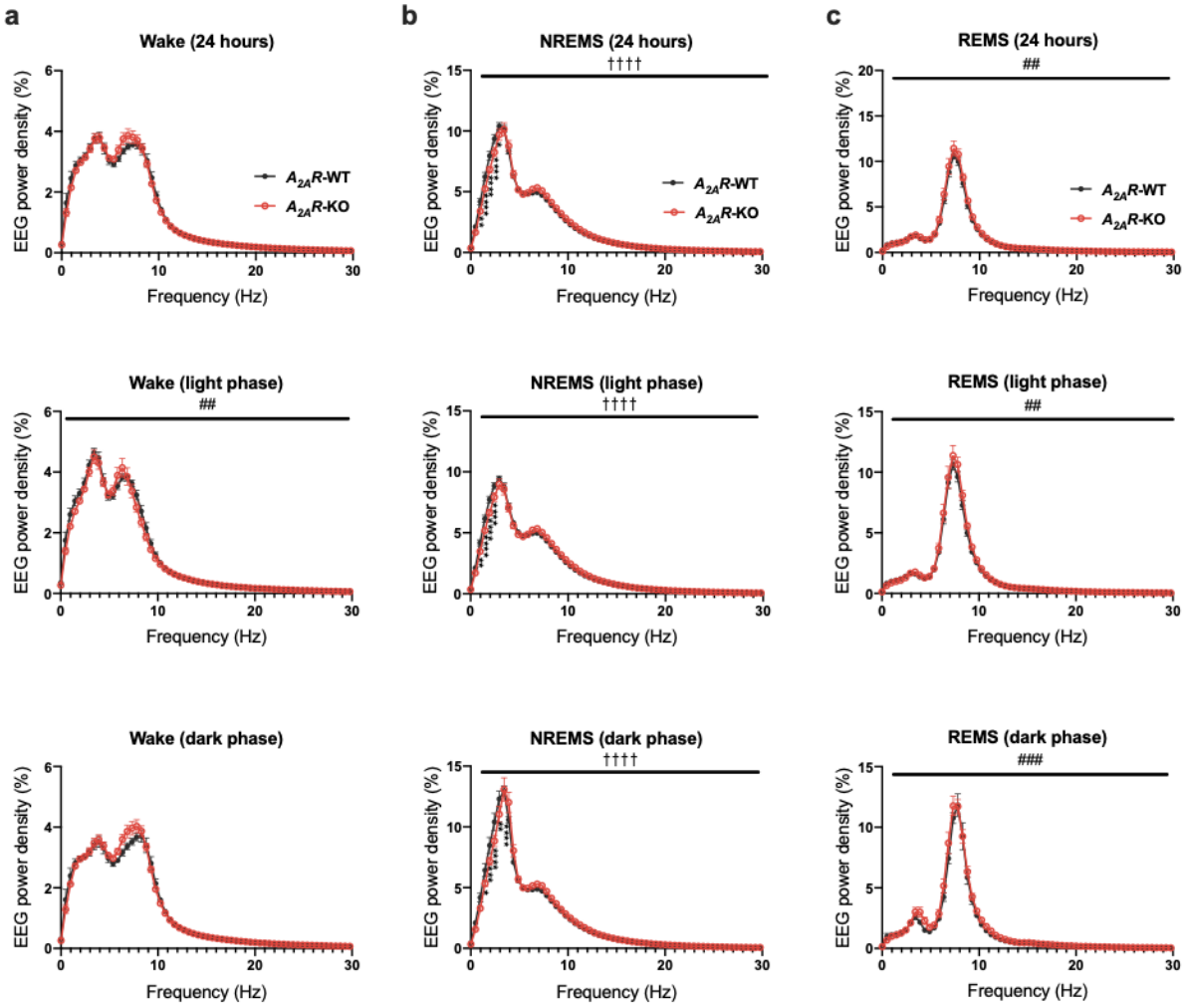

Figure 7. EEG power density during wakefulness, NREM sleep and REM sleep in *$A_{2A}R$* -WT and *$A_{2A}R$*-KO mice.

a-c, Comparison of EEG power density (mean± s.e.m.) during wakefulness (**a**), NREM sleep (**b**) and REM sleep (**c**) for 24 hours, light and dark phases between *$A_{2A}R$* -WT and *$A_{2A}R$*-KO mice (n= 8 male mice for each genotype; number of mice differs from that in Fig. 10 because individuals that exhibited contamination of large noise during wakefulness were excluded). # and † indicate significant main effect of genotype and significant interaction between frequency and genotype, respectively, in two-way ANOVA (## P<0.01; ### P<0.001; †††† P<0.0001). * indicates significance in post-hoc Bonferroni's multiple comparisons test (*P <0.05, **P <0.01, *** P<0.001, **** P <0.0001). Note that the EEG power density of REM sleep in Fig. **11c** was comparing only the REM sleep episodes which duration were longer than 40 seconds, while in Fig. **7**, all length of REM sleep episodes were analyzed.

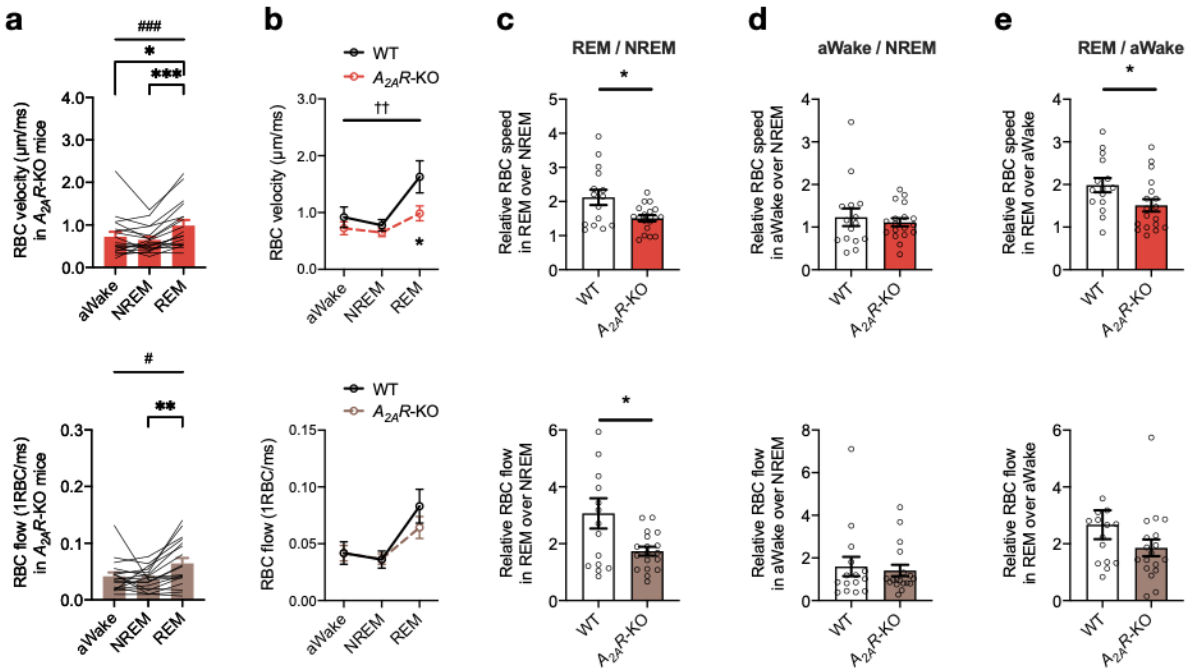

Figure 8. *A_{2A}R*-KO mice exhibited an impairment in the upsurge of CBF during REM sleep.

a, RBC velocity and flow (mean± s.e.m.) in the parietal cortex of *A_{2A}R*-KO mice during active wakefulness, NREM sleep and REM sleep (n=18 capillaries; 8 mice (5 females, 3 males)). # indicates significant effect of sleep/wake state in repeated-measures one-way ANOVA (# P<0.05; ### P<0.001). * indicates significance in the post-hoc Tukey's multiple comparisons test (* P <0.05; ** P <0.01; *** P <0.001). **b,** Comparisons of RBC velocity and flow (mean± s.e.m.) between WT and *A_{2A}R*-KO mice in parietal cortex across the sleep/wake cycle (same data shown in **3c** and **8a**). † indicates significant interaction between genotype and sleep/wake state in repeated-measures two-way ANOVA (†† P <0.01). * indicates significance in post-hoc Sidak's multiple comparisons test (* P <0.05). **c-e** Relative RBC velocity or flow (mean± s.e.m.) during REM sleep **(c)** or active wakefulness **(d)** in terms of ratio over NREM sleep, as well as relative RBC velocity or flow (mean± s.e.m.) of REM sleep over active wakefulness (**e**) in WT and *A_{2A}R*-KO mice. * indicates significance in Welch's test (* P <0.05). Each line in **a** and each open/closed circle in **c-e** represents an individual capillary.

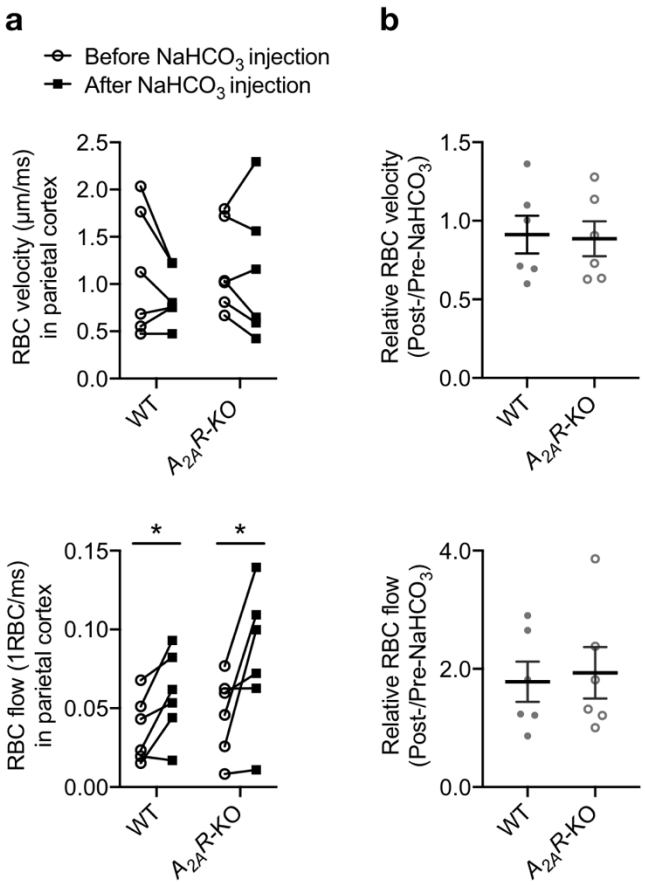

Figure 9. Similar capillary CBF responses to sodium bicarbonate in WT and *A2AR*-KO mice.

a,b, Effects of sodium bicarbonate ($NaHCO_3$) systemic administration on capillary CBF in the parietal cortex in WT and *A2AR*-KO mice. CBF of each capillary before and after $NaHCO_3$ administration was compared (WT: n= 6 capillaries; 2 mice (1 female, 1 male); A_{2A}R-KO: n=6 capillaries; 2 mice (2 females)). Comparisons of absolute RBC velocity and flow are shown in **a**. * indicates significance in paired t test (* P <0.05). For comparison of relative RBC velocity and flow (mean± s.e.m.) in post-$NaHCO_3$ treatment over pre-$NaHCO_3$ treatment (**b**), no significant difference was detected between genotypes (Welch's test). Each line **a** and each open/closed circle in **b** represents an individual capillary. Treatments and 2PM imaging were performed on WT and *A2AR*-KO mice in age of 7-8 month in this figure.

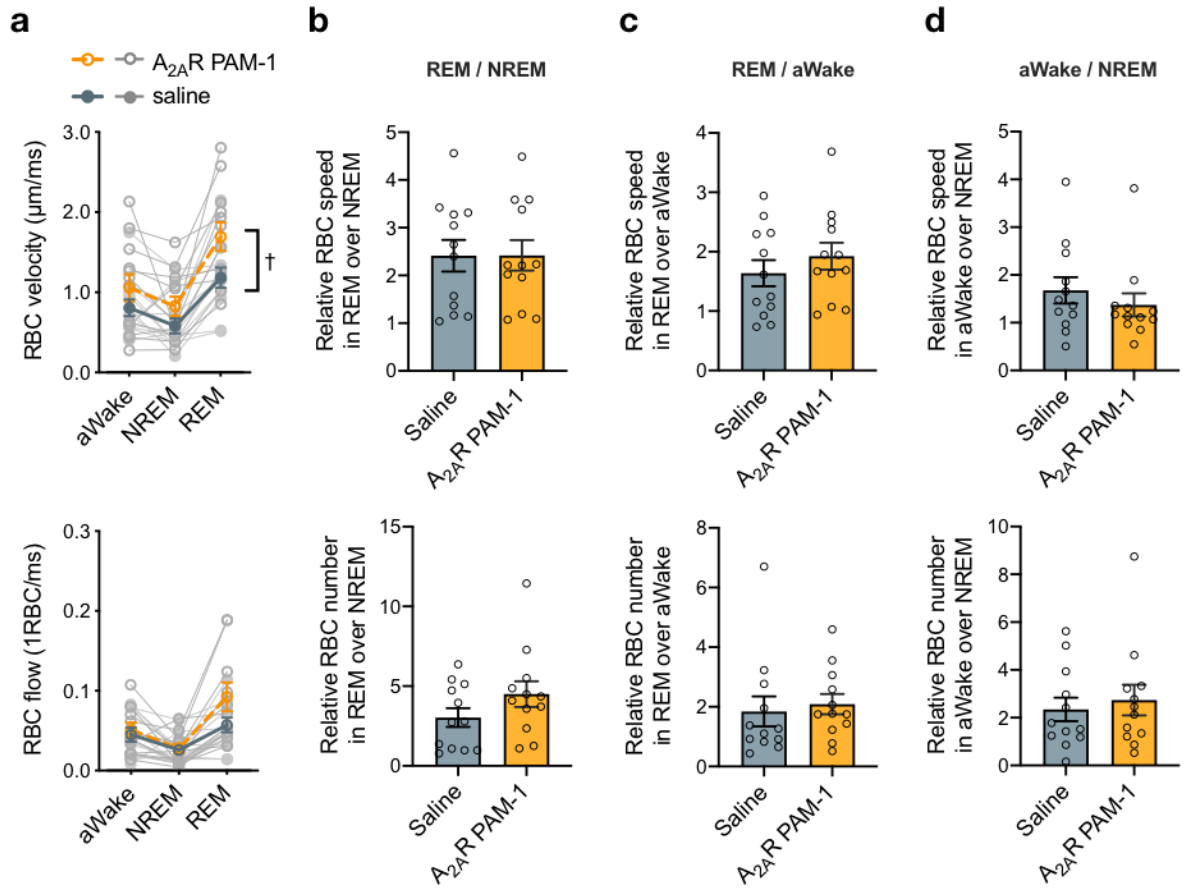

Figure 10. Elevation of RBC velocity across the sleep/wake cycle in response to $A_{2A}R$ positive allosteric modulator in WT mice.

a-d, Effects of $A_{2A}R$ positive allosteric modulator **(**$A_{2A}R$ PAM-1) systemic administration on capillary CBF in parietal cortex ($A_{2A}R$ PAM-1: n= 12 capillaries; 3 mice (3 males); saline: n= 12 capillaries; 3 mice (3 males)). Comparisons of absolute RBC velocity and flow (mean± s.e.m.) across sleep/wake cycles between conditions are shown in **a**. † indicates significant main effect of drug in repeated-measures two-way ANOVA († P <0.05). In comparisons of relative RBC velocity and flow (mean± s.e.m.) during REM sleep **(b)** or active wakefulness **(d)** over NREM sleep, as well as relative RBC velocity or flow (mean± s.e.m.) of REM sleep over active wakefulness (**c**), no significant difference between $A_{2A}R$ PAM-1 and saline treatment groups was detected (Welch's test). Each open circle in **b-d** represents an individual capillary. Treatments and 2PM imaging were performed on WT mice in age of 3-5 month in this figure.

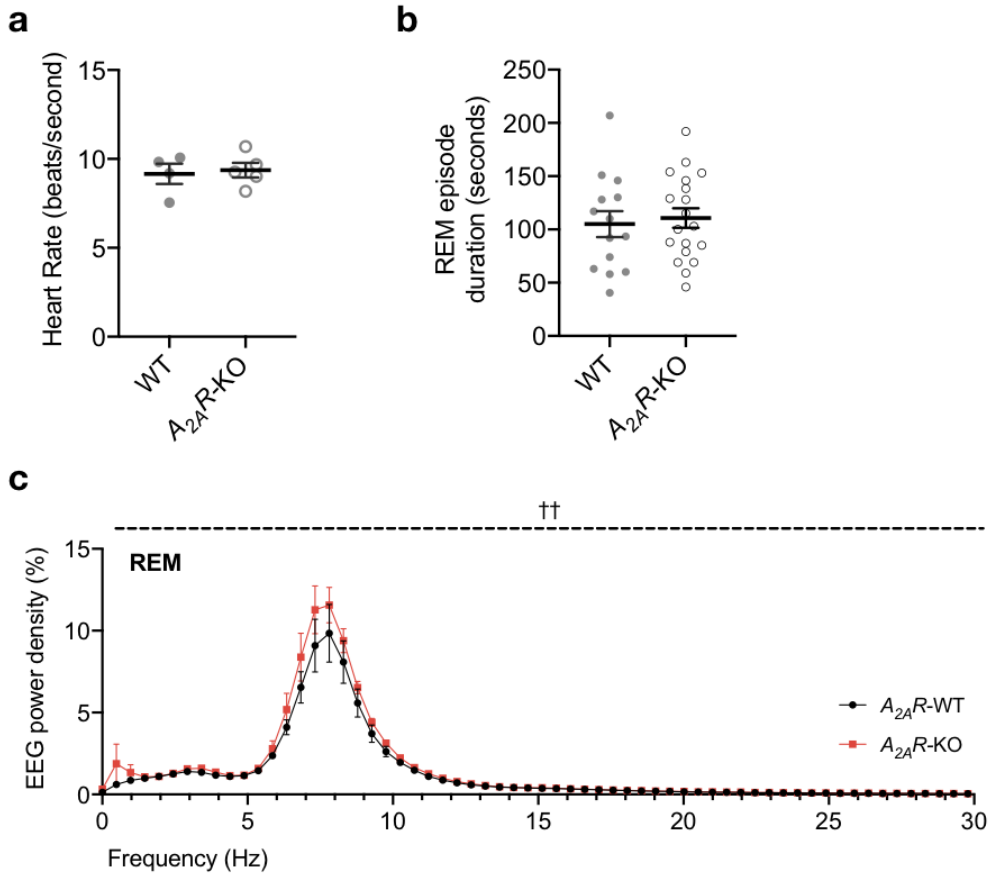

Figure 11. Comparison of various measures of REM sleep (heart rate, episode duration, EEG power spectrum) between WT and *A2AR*-KO mice .

a, Heart rate (mean± s.e.m.) during REM sleep in WT (n=4 mice (2 females, 2 males)) and *A2AR*-KO (n=5 mice (4 females, 1 male)) mice are plotted. Each dot represents an individual mouse. No significant difference between genotypes was detected (Welch's test). **b**, Duration (mean± s.e.m.) of REM sleep episodes from which XT line scans were analyzed in **3c** and **8a** between WT (n=4 mice (2 females, 2 males)) and *A2AR*-KO (n=6 mice (4 females, 2 male)). Each circle represents a single REM sleep episode. No significant difference was detected between genotypes (Welch's test). **c**, REM sleep episodes with durations longer than 40 seconds (roughly corresponding to the minimum duration of REM sleep episodes for collecting CBF data) were analyzed (n=4 male mice for each genotype). Note that the EEG power density of REM sleep in Fig. **7c** was comparing all the REM sleep episodes in spite of its duration. † indicates significant main effect of genotype in repeated-measures two-way ANOVA (†† P <0.01). Each open/closed dot represents an individual mouse (**a**) and individual REM episode (**b**).

REFERENCES

Akgören, N., and Lauritzen, M. (1999). Functional recruitment of red blood cells to rat brain microcirculation accompanying increased neuronal activity in cerebellar cortex. Neuroreport *10*, 3257–3263.

Benington, J.H., Kodali, S.K., and Heller, H.C. (1995). Stimulation of A1 adenosine receptors mimics the electroencephalographic effects of sleep deprivation. Brain Research *692*, 79–85.

Bergel, A., Deffieux, T., Demené, C., Tanter, M., and Cohen, I. (2018). Local hippocampal fast gamma rhythms precede brain-wide hyperemic patterns during spontaneous rodent REM sleep. Nature Communications *9*, 1–12.

Bjorness, T.E., Kelly, C.L., Gao, T., Poffenberger, V., and Greene, R.W. (2009). Control and function of the homeostatic sleep response by adenosine A1 receptors. J. Neurosci. *29*, 1267–1276.

Boyce, R., Glasgow, S.D., Williams, S., and Adamantidis, A. (2016). Causal evidence for the role of REM sleep theta rhythm in contextual memory consolidation. Science *352*, 812–816.

Braun, A.R., Balkin, T.J., Wesenten, N.J., Carson, R.E., Varga, M., Baldwin, P., Selbie, S., Belenky, G., and Herscovitch, P. (1997). Regional cerebral blood flow throughout the sleep-wake cycle. An H2(15)O PET study. Brain *120*, 1173–1197.

Buckley, E.M., Naim, M.Y., Lynch, J.M., Goff, D.A., Schwab, P.J., Diaz, L.K., Nicolson, S.C., Montenegro, L.M., Lavin, N.A., Durduran, T., et al. (2013). Sodium bicarbonate causes dose-dependent increases in cerebral blood flow in infants and children with single-ventricle physiology. Pediatr Res *73*, 668–673.

Campbell, S.S., and Tobler, I. (1984). Animal sleep: A review of sleep duration across phylogeny. Neuroscience and Biobehavioral Reviews *8*, 269–300.

Chaigneau, E., Oheim, M., Audinat, E., and Charpak, S. (2003). Two-photon imaging of capillary blood flow in olfactory bulb glomeruli. Proc. Natl. Acad. Sci. U.S.a. *100*, 13081–13086.

Chauvette, S., Seigneur, J., and Timofeev, I. (2012). Sleep Oscillations in the Thalamocortical System Induce Long-Term Neuronal Plasticity. Neuron *75*, 1105–1113.

Chen, J.F., Huang, Z., Ma, J., Zhu, J., Moratalla, R., Standaert, D., Moskowitz, M.A., Fink, J.S., and Schwarzschild, M.A. (1999). A(2A) adenosine receptor deficiency attenuates brain injury induced by transient focal ischemia in mice. J. Neurosci. *19*, 9192–9200.

Cipolla, M.C.T.C. (2009). Chapter 5 Control of cerebral blood flow. In The Cerebral Circulation, (San Rafael (CA): Morgan & Claypool Life Sciences), pp. 2567–2577.

Cruz Hernández, J.C., Bracko, O., Kersbergen, C.J., Muse, V., Haft-Javaherian, M., Berg, M., Park, L., Vinarcsik, L.K., Ivasyk, I., Rivera, D.A., et al. (2019). Neutrophil adhesion in brain capillaries reduces cortical blood flow and impairs memory function in Alzheimer's disease mouse models. Nat Neurosci *22*, 413–420.

Dukart, J., Holiga, A.X.T., Chatham, C., Hawkins, P., Forsyth, A., McMillan, R., Myers, J., Lingford-Hughes, A.R., Nutt, D.J., Merlo-Pich, E., et al. (2018). Cerebral blood flow predicts differential neurotransmitter activity. Scientific Reports *8*, 1–11.

Dumoulin Bridi, M.C., Aton, S.J., Seibt, J., Renouard, L., Coleman, T., and Frank, M.G. (2015). Rapid eye movement sleep promotes cortical plasticity in the developing brain. Sci Adv *1*, e1500105–e1500109.

Evarts, E.V. (1964). Temporal patterns of discharge of pyramidal tract neurons during sleep and waking in the monkey. Journal of Neurophysiology *27*, 152–171.

Fantini, S., Sassaroli, A., Tgavalekos, K.T., and Kornbluth, J. (2016). Cerebral blood flow and autoregulation: current measurement techniques and prospects for noninvasive optical methods. Neurophotonics *3*, 031411.

Grant, D.A., Grant, D.A., Franzini, C., Franzini, C., Wild, J., Wild, J., of, K.E.T.J., Eede, K.J., Walker, A.M., 2005 (2005). Autoregulation of the cerebral circulation during sleep in newborn lambs. The Journal of Physiology *564*, 923–930.

Gronfier, C., Luthringer, R., Follenius, M., Schaltenbrand, N., Macher, J.P., Muzet, A., and Brandenberger, G. (1996). A quantitative evaluation of the relationships between growth

hormone secretion and delta wave electroencephalographic activity during normal sleep and after enrichment in delta waves. Sleep *19*, 817–824.

Gronfier, C., Luthringer, R., Follenius, M., Schaltenbrand, N., Macher, J.P., Muzet, A., and Brandenberger, G. (1997). Temporal relationships between pulsatile cortisol secretion and electroencephalographic activity during sleep in man. Electroencephalogr Clin Neurophysiol *103*, 405–408.

Guevara-Torres, A., Joseph, A., and Schallek, J.B. (2016). Label free measurement of retinal blood cell flux, velocity, hematocrit and capillary width in the living mouse eye. Biomed. Opt. Express *7*, 4228–22.

Hayashi, Y., Kashiwagi, M., Yasuda, K., Ando, R., Kanuka, M., Sakai, K., and Itohara, S. (2015). Cells of a common developmental origin regulate REM/non-REM sleep and wakefulness in mice. Science *350*, 957–961.

Hoffmann, C., Gaietta, G., Bünemann, M., Adams, S.R., Oberdorff-Maass, S., Behr, B., Vilardaga, J.-P., Tsien, R.Y., Ellisman, M.H., and Lohse, M.J. (2005). A FlAsH-based FRET approach to determine G protein–coupled receptor activation in living cells. Nat Meth *2*, 171–176.

Holtmaat, A., Bonhoeffer, T., Chow, D.K., Chuckowree, J., De Paola, V., Hofer, S.B., Hübener, M., Keck, T., Knott, G., Lee, W.-C.A., et al. (2009). Long-term, high-resolution imaging in the mouse neocortex through a chronic cranial window. Nat Protoc *4*, 1128–1144.

Hossmann, K.A. (1994). Viability thresholds and the penumbra of focal ischemia. Annals of Neurology *36*, 557–565.

Huang, Z.-L., Qu, W.-M., Eguchi, N., Chen, J.-F., Schwarzschild, M.A., Fredholm, B.B., Urade, Y., and Hayaishi, O. (2005). Adenosine A2A, but not A1, receptors mediate the arousal effect of caffeine. Nat Neurosci *8*, 858–859.

Iliff, J.J., Wang, M., Zeppenfeld, D.M., Venkataraman, A., Plog, B.A., Liao, Y., Deane, R., and Nedergaard, M. (2013). Cerebral arterial pulsation drives paravascular CSF-interstitial fluid exchange in the murine brain. J. Neurosci. *33*, 18190–18199.

Kisler, K., Nelson, A.R., Montagne, A., and Zlokovic, B.V. (2017). Cerebral blood flow regulation and neurovascular dysfunction in Alzheimer disease. Acta Pharmacol. Sin. *18*, 419–434.

Kleinfeld, D., Mitra, P.P., Helmchen, F., and Denk, W. (1998). Fluctuations and stimulus-induced changes in blood flow observed in individual capillaries in layers 2 through 4 of rat neocortex. Proc. Natl. Acad. Sci. U.S.a. *95*, 15741–15746.

Korkutata, M., Saitoh, T., Cherasse, Y., Ioka, S., Duo, F., Qin, R., Murakoshi, N., Fujii, S., Zhou, X., Sugiyama, F., et al. (2019). Enhancing endogenous adenosine A2A receptor signaling induces slow-wave sleep without affecting body temperature and cardiovascular function. Neuropharmacology *144*, 122–132.

Kubota, Y., Takasu, N.N., Horita, S., Kondo, M., Shimizu, M., Okada, T., Wakamura, T., and Toichi, M. (2011). Dorsolateral prefrontal cortical oxygenation during REM sleep in humans. Brain Research *1389*, 83–92.

Lecoq, J., Parpaleix, A., Roussakis, E., Ducros, M., Goulam Houssen, Y., Vinogradov, S.A., and Charpak, S. (2011). Simultaneous two-photon imaging of oxygen and blood flow in deep cerebral vessels. Nat Med *17*, 893–898.

Li, W., Ma, L., Yang, G., and Gan, W.-B. (2017). REM sleep selectively prunes and maintains new synapses in development and learning. Nat Neurosci *20*, 427–437.

Louveau, A., Smirnov, I., Keyes, T.J., Eccles, J.D., Rouhani, S.J., Peske, J.D., Derecki, N.C., Castle, D., Mandell, J.W., Lee, K.S., et al. (2015). Structural and functional features of central nervous system lymphatic vessels. Nature *523*, 337–341.

Lydic, R., and Baghdoyan, H.A. (1993). Pedunculopontine stimulation alters respiration and increases ACh release in the pontine reticular formation. Am. J. Physiol. *264*, R544–R554.

Maloney, K.J., Mainville, L., and Jones, B.E. (1999). Differential c-Fos expression in cholinergic, monoaminergic, and GABAergic cell groups of the pontomesencephalic tegmentum after paradoxical sleep deprivation and recovery. J. Neurosci. *19*, 3057–3072.

Maquet, P., Dive, D., Salmon, E., Sadzot, B., Franco, G., Poirrier, R., Frenckell, von, R., and Franck, G. (1990). Cerebral glucose utilization during sleep-wake cycle in man determined

by positron emission tomography and [18F]2-fluoro-2-deoxy-d-glucose method. Brain Research *513*, 136–143.

Marrosu, F., Portas, C., Mascia, M.S., Casu, M.A., Fà, M., Giagheddu, M., Imperato, A., and Gessa, G.L. (1995). Microdialysis measurement of cortical and hippocampal acetylcholine release during sleep-wake cycle in freely moving cats. Brain Research *671*, 329–332.

McAvoy, M.P., Tagliazucchi, E., Laufs, H., and Raichle, M.E. (2018). Human non-REM sleep and the mean global BOLD signal. J Cereb Blood Flow Metab *19*, 0271678X1879107–X1879113.

Mesquita, S., Louveau, A., Vaccari, A., Smirnov, I., Cornelison, R.C., Kingsmore, K.M., Contarino, C., Onengut-Gumuscu, S., Farber, E., Raper, D., et al. (2018). Functional aspects of meningeal lymphatics in ageing and Alzheimer's disease. Nature *560*, 1–32.

Mileykovskiy, B.Y., Kiyashchenko, L.I., and Siegel, J.M. (2005). Behavioral Correlates of Activity in Identified Hypocretin/Orexin Neurons. Neuron *46*, 787–798.

Miyamoto, D., Hirai, D., Fung, C.C.A., Inutsuka, A., Odagawa, M., Suzuki, T., Boehringer, R., Adaikkan, C., Matsubara, C., Matsuki, N., et al. (2016). Top-down cortical input during NREM sleep consolidates perceptual memory. Science *352*, 1315–1318.

Miyazaki, S., Liu, C.-Y., and Hayashi, Y. (2017). Sleep in vertebrate and invertebrate animals, and insights into the function and evolution of sleep. Neuroscience Research *118*, 3–12.

Monti, J.M. (2013). The neurotransmitters of sleep and wake, a physiological reviews series. Sleep Medicine Reviews *17*, 313–315.

Nagayama, M., Aritake, T., Hino, H., Kanda, T., Miyazaki, T., Yanagisawa, M., Akaho, S., and Murata, N. (2019). Sleep State Analysis Using Calcium Imaging Data by Non-negative Matrix Factorization. In Artificial Neural Networks and Machine Learning – ICANN 2019: Theoretical Neural Computation, (Cham: Springer, Cham), pp. 102–113.

Ngai, A.C., Coyne, E.F., Meno, J.R., West, G.A., and Winn, H.R. (2001). Receptor subtypes mediating adenosine-induced dilation of cerebral arterioles. Am. J. Physiol. Heart Circ. Physiol. *280*, H2329–H2335.

Norimoto, H., Makino, K., Gao, M., Shikano, Y., Okamoto, K., Ishikawa, T., Sasaki, T., Hioki, H., Fujisawa, S., and Ikegaya, Y. (2018). Hippocampal ripples down-regulate synapses. Science *359*, 1524–1527.

Parpaleix, A., Goulam Houssen, Y., and Charpak, S. (2013). Imaging local neuronal activity by monitoring PO_2 transients in capillaries. Nat Med *19*, 241–246.

Pase, M.P., Himali, J.J., Grima, N.A., Beiser, A.S., Satizabal, C.L., Aparicio, H.J., Thomas, R.J., Gottlieb, D.J., Auerbach, S.H., and Seshadri, S. (2017). Sleep architecture and the risk of incident dementia in the community. Neurology *89*, 1244–1250.

Paulson, O.B., Strandgaard, S., and Edvinsson, L. (1990). Cerebral autoregulation. Cerebrovasc Brain Metab Rev *2*, 161–192.

Porkka-Heiskanen, T., Strecker, R.E., Thakkar, M., Bjorkum, A.A., Greene, R.W., and McCarley, R.W. (1997). Adenosine: a mediator of the sleep-inducing effects of prolonged wakefulness. Science *276*, 1265–1268.

Rasch, B., Büchel, C., Gais, S., and Born, J. (2007). Odor cues during slow-wave sleep prompt declarative memory consolidation. Science *315*, 1426–1429.

Rial, R.V., rir, M.A., GamundÃ, A., Nicolau, C., Garau, C., Aparicio, S., Tejada, S., GenÃ, L., lez, J.N.G., De Vera, L.M., et al. (2010). Evolution of wakefulness, sleep and hibernation: From reptiles to mammals. Neuroscience and Biobehavioral Reviews *34*, 1144–1160.

Roome, C.J., and Kuhn, B. (2014). Chronic cranial window with access port for repeated cellular manipulations, drug application, and electrophysiology. Front Cell Neurosci *8*, 379.

Roux, L., Hu, B., Eichler, R., Stark, E., and Buzsáki, G. (2017). Sharp wave ripples during learning stabilize the hippocampal spatial map. Nat Neurosci *20*, 845–853.

Sweeney, M.D., Kisler, K., Montagne, A., Toga, A.W., and Zlokovic, B.V. (2018). The role of brain vasculature in neurodegenerative disorders. Nat Neurosci *21*, 1–14.

Takahashi, Y., Kipnis, D.M., and Daughaday, W.H. (1968). Growth hormone secretion during sleep. J. Clin. Invest. *47*, 2079–2090.

Thakkar, M., Portas, C., and McCarley, R.W. (1996). Chronic low-amplitude electrical stimulation of the laterodorsal tegmental nucleus of freely moving cats increases REM sleep. Brain Research *723*, 223–227.

Verret, L., Fort, P., Gervasoni, D., Léger, L., and Luppi, P.-H. (2006). Localization of the neurons active during paradoxical (REM) sleep and projecting to the locus coeruleus noradrenergic neurons in the rat. J. Comp. Neurol. *495*, 573–586.

Watson, B.O., Levenstein, D., Greene, J.P., Gelinas, J.N., and Buzsáki, G. (2016). Network Homeostasis and State Dynamics of Neocortical Sleep. *90*, 839–852.

Watson, C.J., Baghdoyan, H.A., and Lydic, R. (2010). Neuropharmacology of Sleep and Wakefulness. Sleep Med Clin *5*, 513–528.

Wei, H.S., Kang, H., Rasheed, I.-Y.D., Zhou, S., Lou, N., Gershteyn, A., McConnell, E.D., Wang, Y., Richardson, K.E., Palmer, A.F., et al. (2016). Erythrocytes Are Oxygen-Sensing Regulators of the Cerebral Microcirculation. Neuron *91*, 851–862.

Xie, L., Kang, H., Xu, Q., Chen, M.J., Liao, Y., Thiyagarajan, M., O'Donnell, J., Christensen, D.J., Nicholson, C., Iliff, J.J., et al. (2013a). Sleep Drives Metabolite Clearance from the Adult Brain. Science *342*, 373–377.

Xie, L., Kang, H., Xu, Q., Chen, M.J., Liao, Y., Thiyagarajan, M., O'Donnell, J., Christensen, D.J., Nicholson, C., Iliff, J.J., et al. (2013b). Sleep drives metabolite clearance from the adult brain. Science *342*, 373–377.

Yang, G., Lai, C.S.W., Cichon, J., Ma, L., Li, W., and Gan, W.-B. (2014). Sleep promotes branch-specific formation of dendritic spines after learning. Science *344*, 1173–1178.

Yoon, S., Zuccarello, M., and Rapoport, R.M. (2012). pCO(2) and pH regulation of cerebral blood flow. Front Physiol *3*, 365.